Neurocomputing 186 (2016) 207–217

Contents lists available at ScienceDirect

Neurocomputing

journal homepage: www.elsevier.com/locate/neucom

Biological modeling the undulatory locomotion of *C. elegans* using dynamic neural network approach

Xin Deng [a,b], Jian-Xin Xu [b], Jin Wang [a,*], Guo-yin Wang [a], Qiao-song Chen [a]

[a] Chongqing Key Laboratory of Computational Intelligence, Chongqing University of Posts and Telecommunications, Nan'an District, Chongqing 400065, China

[b] National University of Singapore, 117576, Singapore

ARTICLE INFO

Article history:
Received 28 October 2015
Received in revised form
23 December 2015
Accepted 25 December 2015
Communicated by W.L. Dunin-Barkowski
Available online 8 January 2016

Keywords:
Undulatory locomotion
Dynamic neural networks
C. elegans

ABSTRACT

This paper provides an undulatory locomotion model of *C. elegans* to achieve the chemotaxis behaviors based on the biological neuronal and neuromuscular structure. The *on-cell* and *off-cell* mechanism, as well as the proprioceptive mechanism is incorporated into the locomotion model. The nervous system of *C. elegans* is modeled by a dynamic neural network (DNN) that involves two parts: head DNN and motor neurons. The head DNN perceives the outside concentrations and generates the undulatory wave to the body. The motor neurons are responsible for transiting the undulatory wave along the body. The body of *C. elegans* is represented as a multi-joint rigid link model with 11 links. The undulatory locomotion behavior is achieved by using the DNN to control the lengths of muscles on ventral and dorsal sides, and then using the muscle lengths to control the angles between two consecutive links. In this work, the relations between the outputs of DNN and muscle lengths, as well as the muscle lengths and the angles between two consecutive links, are determined. Furthermore, owing to the learning capability of DNN, a set of nonlinear functions that are designed to represent the chemotaxis behaviors of *C. elegans* are learned by the head DNN. The testing results show good performance of the locomotion model for the chemotaxis behaviors of finding food and avoiding toxin, as well as slight and Ω turns. At last, quantitative analyses by comparing with the experiment results are provided to verify the realness and effectiveness of the locomotion model, which could serve as a prototype for other footless animals.

1. Introduction

Undulatory locomotion is one of the fundamental behaviors of the footless animals, such as larva, worm, snake, and even some mammals. Among these animals, the snake has been widely studied to disclose the mechanism of undulatory motion. However, due to the huge amount of neurons and muscle–bone structures of the snake, it is difficult to study the motion mechanism from the cellular level. Fortunately, *C. elegans* offers us an idea model to study the mechanism of undulatory locomotion behavior. The nervous system of *C. elegans* contains 302 neurons and 95 muscles, and all the neuronal connections are visibly known [1]. The undulatory locomotion of *C. elegans* is similar to other limbless animals, such as snake, and the neural circuit of *C. elegans* is much simpler than that of snake. So the clearly described nervous and muscular systems of *C. elegans* provide us a good opportunity to investigate the essence of undulatory locomotion from the cellular level. Furthermore, if we realize these mechanisms on the computer, it may be possible to incorporate these biological or biomimetic methods into the undulatory robots, which can achieve at least four tasks: (1) rescuing survivors in complex areas where human cannot enter [2]; (2) checking the inner side of the industrial equipment pipes [3]; (3) crawling on the ground, under water, or inside the pipes for military utilities [4,5]; (4) checking the stomach, blood vessels, or intestine for clinical use [6].

The study of undulatory locomotion behavior of *C. elegans* began in recent years. Suzuki et al. explored the locomotion behaviors of *C. elegans* in forward movement, backward movement, and turning [7–10]. Boyle et al. investigated how the muscles and neurons of *C. elegans* created the *S* wave and how it was propagated from the head to tail [11,12]. They also designed and constructed a giant worm-like robot based on the proprioception mechanism of *C. elegans* [13]. In the work of Karbowski et al. [14], a locomotion model was constructed based on the experimental results. Their computational model can predict the mechanisms underlying various behaviors of mutant *C. elegans*. Furthermore,

* Corresponding author.
E-mail addresses: dengxin@cqupt.edu.cn (X. Deng), wangjin@cqupt.edu.cn (J. Wang).

http://dx.doi.org/10.1016/j.neucom.2015.12.090
0925-2312/

Mailler et al. constructed a 3D locomotion model of *C. elegans* [15]. The body of this 3D model was assembled by 25 boxes and the muscles were represented by springs. Without preserving the biological anatomical structure, the locomotion behavior of the 3D model was displayed mainly in the game engine, and no precise mathematical description was given. Yuk et al. constructed two robots to mimic the undulatory behavior of *C. elegans* by using the Shape Memory Alloy [16,17]. Xu and Deng used the dynamic neural network to mimic the chemotaxis behavior of *C. elegans* [18] and explore the speed regulation mechanism [19]. They also constructed a 3D locomotion model to investigate the undulatory locomotion [20]. In a recent paper, Portegys trained the sensory-motor behavior of an artificial *C. elegans* using an evolutionary computing method [21].

The work in this paper is different from the existing work by incorporating the two latest biological outcomes. One is the mechanism of *on-cell* and *off-cell* for the sensory neurons [22–24], and the other is the proprioceptive mechanism between the motor neurons and muscles that propagate the undulatory wave [25]. *On-cell* is the sensory neuron that only actives when outside stimulus increases, whereas *off-cell* only actives when outside stimulus decreases. The mechanisms of *on-cell* and *off-cell* achieve the decision making function for chemotaxis of *C. elegans*. The simplest case is the going or turning behaviors, for which the presence or absence of the behavior under investigation is dictated by the presence or absence of the stimulus. For instance, it is well-known that ASEL is *on-cell* and ASER is *off-cell* for attractant [22]. To find food, the positive gradient food concentration makes ASEL active to inhibit the turning behavior, whereas the negative gradient food concentration makes ASEH active to initiate the turning behavior.

The proprioceptive coupling between muscles and motor neurons is a recent explanation to address the mechanism of undulatory wave propagation of *C. elegans*. Previously, researchers believed that the body wall muscles of *C. elegans* were electrically coupled by gap junctions and appeared to propagate the undulatory wave independently of the nervous system, which was similar to a related nematode, *Ascaris* [26]. However, two latest experimental results indicate that the gap junctions between muscles are insufficient to propagate bending signal between neighboring body regions [12,25]. Without using the muscles alone, another choice for the wave propagation is the motor neurons since they are connected by gap junctions. However, by checking the biological wire diagram, the motor neurons are not fully connected [27]. So it is still a problem by using the motor neurons alone to propagate the undulatory wave. Consequently, the proprioceptive mechanism appears to interpret this issue. It claims that except for a circuit near the head that generates the undulatory wave of the most anterior segment, the proprioceptive coupling between muscles and motor neurons also can generate and propagate the undulatory wave. The bending of one body region requires the bending of its anterior neighbor. In other words, the muscle activity is positively correlated with the curvature of adjacent anterior neighbors. B-type motor neurons are directly responsible for this proprioceptive coupling. The phase lag of undulatory wave is produced by the neuromuscular delay, which is yielded by the synaptic transmission and the limiting speed of muscle contraction.

Besides two mechanisms mentioned above, the novelties and uniqueness of this work include other four aspects. First, we construct the undulatory locomotion model of *C. elegans* based on the biological structure instead of artificial structure. The undulatory locomotion model is divided into three parts: head part, motor neurons part, and muscular system, which follow the biological neuronal and neuromuscular connections. Second, the nervous system of *C. elegans* for our model is represented by a DNN, and each neuron is described as a non-linear active function. DNN is a kind of neural networks that owns the dynamic feature compared with the static neural networks (Feed-forward Neural Networks, SOM, RBF, etc.). It is inspired from biological control systems and each neuron is depicted by the dynamic equations [28]. The dynamical feature of DNN makes it more analogous to the nature of nervous system such as the neuronal states changing and so on. Furthermore, it is also suitable for chemotaxis behavioral modeling owing to its dynamical nature that its connections can be made analogous to the nature ones such as synapses. DNN for the head part is to smell the outside concentration and make the decision of turning. Additionally, a circuit to produce the undulatory wave is contained in the head DNN. DNN for the motor neurons part and muscles system are responsible for propagating the undulatory wave along the body using a proprioceptive mechanism. Third, the muscles are modeled to associate with the outputs of DNN. When receiving the undulatory wave from the DNN, the length of muscle will change according to the magnitude of signal and the body shape will also change accordingly. In this way, we can use the outputs of DNN to control the shape of *C. elegans*. Fourth, with the strong learning capability of DNN, our model can implement the chemotaxis behaviors of finding food and avoiding toxin concurrently after the head DNN learning a set of nonlinear functions. These nonlinear functions, which are called switch logic functions (SLFs), are designed based on the fuzzy logic to approximate the logic of *C. elegans* during chemotaxis locomotion. Once SLFs are learned well, our model can perform the chemotaxis behaviors in different simulated environments. Furthermore, we also quantitatively analyze the trajectories of our model by comparing with the experimental results and simplify the well optimized head DNN to be smaller ones, by which two patterns are found.

This paper is organized as follows: Section 2 provides the biological structure of *C. elegans* including head part, motor neuron part and muscular system. Section 3 discusses the method to model the sensory neurons, neurons for wave generation, and interneurons. In Section 4, the method of modeling the muscle system is provided in detail. In Section 5, the methods to optimize the whole locomotion model are investigated. Section 6 provides the testing results and Section 7 concludes this work.

2. Wire diagram

In this work, we model the undulatory behavior of *C. elegans* based on its chemotaxis behavior, which is one of the fundamental surviving skills. The wire diagram of *C. elegans* for the chemotaxis behavior is extracted based on the data provided by [29,30]. We fix the sensory neuron ASER and ASEL as input neurons for food attraction, ASH as input neuron for toxin avoidance [31], and motor neurons as the output neurons. Other interneurons are added by two rules from input neurons to output neurons: with the shortest paths and with the strongest synaptic connections. The chemical synapse from one neuron to another is modeled as a unidirectional connection, and the gap junction between two neurons is modeled as a bidirectional connection with two weights. If both synapses and gap junction exist between two neurons, we still model the wire diagram as a bidirectional connection with two weights. Whether the weights are positive (excitatory) or negative (inhibitory) is determined by training.

2.1. Head DNN

The head DNN is shown in Fig. 1. Three sensory neurons (ellipses), ASEL, ASER, and ASH, function as input neurons. AVD, AVB, AVA, and PVC are four command neurons (diamonds). Six

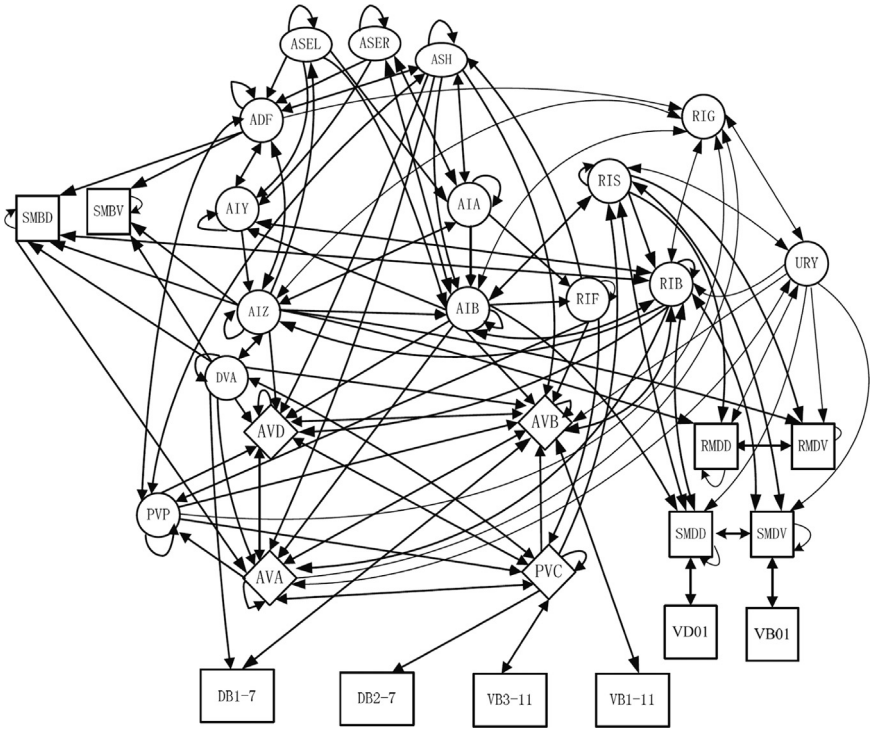

Fig. 1. Head wire diagram. Three ellipses represent the sensory neurons. Circles represent the interneurons. Diamonds represent the command neurons. Rectangles represent the motor neurons.

motor neurons, RMD(D/V), SMB(D/V), and SMD(D/V), control the head and neck muscles and play the critical role in undulatory locomotion [32]. Twelve circles indicate the interneurons, and VB_i ($i=1\ldots11$) and DB_i ($i=1\ldots7$) are motor neurons.

The head wire diagram is to achieve the decision making function for chemotaxis, and it also controls the oscillation of muscles in the head and neck. The contents about modeling the head wire diagram will be discussed in Section 3.

2.2. Motor neurons and muscles

The wire diagram of motor neurons and muscular system are shown in Fig. 2(a). The command neuron AVB connects to VB_i ($i=1\ldots11$) and DB_i ($i=1\ldots7$), and PVC connects VB_i ($i=3\ldots11$) and DB_i ($i=2\ldots7$). The interneuron DVA has the connections to DB_i ($i=1\ldots7$) but does not have the connection to the ventral side motor neurons VB_i ($i=1\ldots11$). Six motor neurons, SMD(D/V), SMB (D/V) and SMD(D/V) that control the head and neck muscles do not connect the command neurons AVB and PVC, but they receive the synaptic inputs from head interneurons, as shown in Fig. 1. Each motor neuron (DB, DD, VB, VD) has the connection to muscles. VB and DB controlled by the command neurons (AVB and PVC) activate the muscles, whereas VD and DD receiving the signals from VB and DB inhibit the muscles. It is interesting that motor neurons in the same group are not fully connected. For instance, VB_7 and VB_8 are not connected between segments 8 and 9, where the vulva exists anatomically. This disconnection supports the hypothesis that the motor neurons alone are not the primary organs to propagate the undulatory wave along the body [25,33]. The method to generate and propagate the undulatory wave by muscles and motor neurons will be discussed in Section 3.

3. Neuron modeling

3.1. Sensory neurons

There exists two types of sensory neurons of *C. elegans* for the chemotaxis behaviors: *on-cell* and *off-cell*. It is well known that ASEL is the *on-cell* and ASER is the *off-cell* [22]. In our work, we adopt the sensory neuron model from [23].

$$V_{on}=\sigma_s(D(t)), \tag{1}$$

$$V_{off}=\sigma_s(-D(t)), \tag{2}$$

where V_{on} is the voltage of *on-cell* and V_{off} is the voltage of the *off-cell*. $D(t)=C_N(t)-C_M(t)$, where $C_N(t)$ is the average concentration over the contiguous interval $[t-N,t]$, and $C_M(t)$ is the average concentration over the interval $[t-(N+M),t-N]$. N and M are the durations of the two intervals. $\sigma_s(\cdot)$ is the activation function

$$\sigma_s(x)=\frac{A}{1+\exp(-k_s(x+x_0))}, \tag{3}$$

where A is the amplitude, and k_s controls the steepness, and the threshold x_0 is a constant. According to Eqs. (1)–(3)**?**, these sensory neurons can compute the temporal concentration difference by themselves. The activations of *on-cell* and *off-cell* following the temporal concentration difference are shown in Fig. 3. The output of *on-cell* (solid line) is positive when $D(t)$ (temporal concentration difference) is greater than 0. Otherwise it maintains to be 0. *off-cell* (dashed line) has the opposite logic to *on-cell*.

Besides the sensory neurons ASEL and ASER are responsible for the attractant (food), the sensory neuron ASH is responsible for the repellent source (toxin). Once *C. elegans* smells the repellent concentration, ASH will be activated to initiate the turning behavior such as slight turn or Ω turn. The activation function for ASH is

$$V_{ASH}=\sigma_{ASH}(C_{tx}(t)), \tag{4}$$

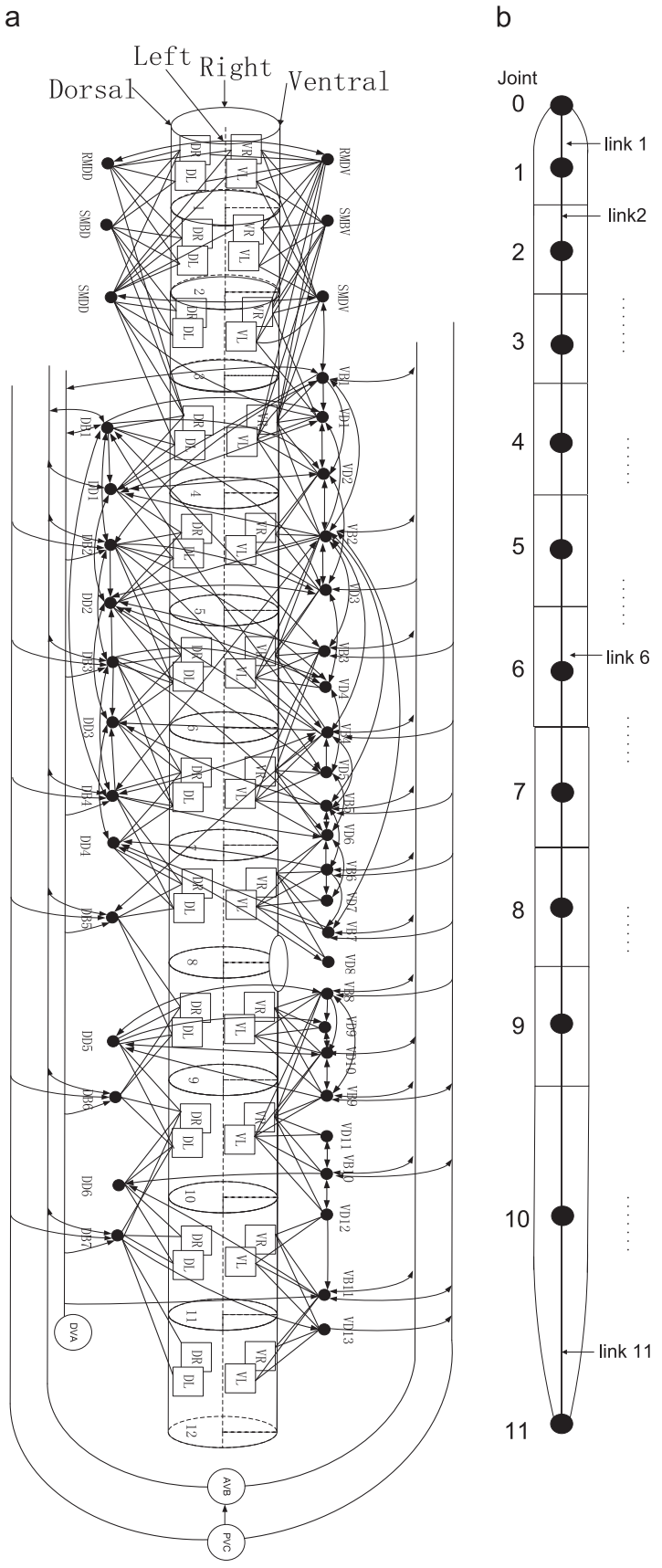

Fig. 2. (a) Wire diagram of motor neurons and neuromuscular connections of *C. elegans*. (b) Multi-joint rigid link system to represent the body of *C. elegans*.

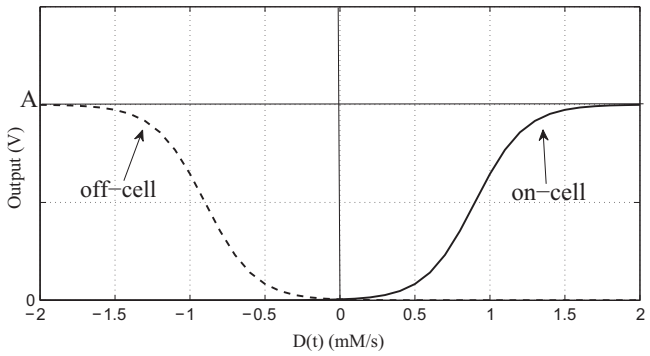

Fig. 3. Activations of *on-cell* and *off-cell* according to temporal concentration difference.

where $C_{tx}(t)$ is the toxin concentration, and $\sigma_{ASH}(\cdot)$ is the activation function having the same form and parameter setting as Eq. (3). ASH serves as the *on-cell* in this work.

3.2. Neurons for undulatory wave generation

The mechanism to generate the undulatory wave is a critical issue for the locomotion of *C. elegans*. It is claimed that there should be a pattern generator near the head to generate the rhythmic bending of the most anterior segment of *C. elegans* [25]. The research work of [14] found that there existed two potential circuits in the head to generate the undulatory wave: AIZ–AIA–AWA–AIZ and RIB–RIG–URY–RIB. Biologically, AIZ, AIA, and AWA have the specific functions that are not suitable for the undulatory wave generation [34–38]. Thus in our model we adopt the last choice, using neurons RIB, RIG, and URY to generate the undulatory wave.

The circuit to generate the undulatory wave is modeled as

$$\tau_b \dot{V}_b = A_b V_b, \tag{5}$$

where

$$\tau_b = \begin{bmatrix} \tau_{RIG} & 0 & 0 \\ 0 & \tau_{RIB} & 0 \\ 0 & 0 & \tau_{URY} \end{bmatrix}, \tag{6}$$

$$A_b = \begin{bmatrix} 0 & -2\pi & 0 \\ 2\pi & 0 & 0 \\ 1 & 0 & -1 \end{bmatrix}, \tag{7}$$

$$V_b = \begin{bmatrix} V_{RIG} \\ V_{RIB} \\ V_{URY} \end{bmatrix}. \tag{8}$$

By choosing the initial values $V_{RIG}(0)=1$, $V_{RIB}(0)=0$, and $\tau_{RIG}=\tau_{RIB}$, the inner periodic signal generators V_{RIG} and V_{RIB} can produce co-sinusoidal signals, $V_{RIG}=\cos(\omega t)$ and $V_{RIB}=\sin(\omega t)$, where $\omega=2\pi/\tau_{RIG}$. V_{URY} can generate either $\cos(\omega t)$ or $\sin(\omega t)$ wave by adjusting τ_{URY}.

3.3. Interneurons

Except three sensory neurons and three neurons for undulatory wave generation, other interneurons in the head DNN are modeled by following Xu et al. [20],

$$\tau_i \frac{dV_i(t)}{dt} = -V_i(t) + \beta_i \tanh\left(\sum_{j=1, j\neq i}^{N} w_{ij}(V_j(t)-\overline{V}_j)\right) + b_i + \delta_i C(t), \tag{9}$$

where τ_i is the time constant that controls the time delay. $V_i(t)$ is the voltage of neuron i at time t. $V_j(t)$ is the voltage of input neuron j. w_{ij} is the connection weight from neuron j to i. The constant $\overline{V}_j$ is the center of the conductance of the jth neuron, which means at this voltage there is no transmitter released from the jth neuron. b_i is a constant bias introduced here to adjust the resting potential value. $\delta_i=1$ if the neuron i is the sensor neuron, otherwise $\delta_i=0$. β_i is a constant that should be determined.

3.4. Motor neurons

The connection of motor neurons is shown in Fig. 2(a). B-type neurons are activation neurons, whereas D-type neurons are inhibition neurons. The motor neurons are not spiking neurons [39] and they receive the feedback of body shape to generate the undulatory wave and propel it forward or backward [25,33,40]. This feedback mechanism is called proprioception, and the proprioceptive coupling between neurons and muscles is transduced by B-type motor neurons [25]. Biologically, the bending of anterior segment directly determines the activity of posterior B-type motor neurons and the potential of B-type neuron positively determines the activities of its connected muscles [25]. In other words, during forward movement the bending of anterior body regions dictates the bending of posterior body regions. B-type neurons are modeled by following [40]:

$$C_B \frac{dV_B}{dt} = -G_B(V_B - E_{rev}) - I_{shape} + I_{AVB}, \tag{10}$$

where C_B is the cell's membrane capacitance; E_{rev} is the cell's effective reversal potential; G_B is the total effective membrane conductance. For motor neuron i, $I_{shape,i}=\sum_{j=1}^{n} w_{ij}^{pro}\sigma_j^{pro}(l_j)$ is the proprioceptive feedback from the shape of its connected muscles. w_{ij}^{pro} is the proprioception weight from muscle j to motor neuron i. l_j is the length of muscle in segment j. $\sigma_j^{pro}(\cdot)$ is a sigmoid function

$$\sigma^{pro}(l) = \frac{A_p}{1+\exp(-k_p(l-l_0))} + b_p, \tag{11}$$

where the steepness parameter k_p and the threshold l_0 are two constants. In Eq. (10), $I_{AVB}=G_{AVB}(V_{AVB}-V_B)$ is the command neuron input. AVB in our model functions as switching on or off the motor neurons for forward locomotion.

For D-type motor neurons, we use the model in [40] directly.

$$C_D \frac{dV_D}{dt} = -G_D(V_D - E_{rev}) - I_{syn}, \tag{12}$$

where $I_{syn}=\sigma_D(V_{pre})$ is the synaptic input from B-type neurons. V_{pre} is the summation of the presynaptic voltages and $\sigma_D(V_{pre})$ is the sigmoid function that has the same form and parameter setting as Eq. (11).

4. Muscle modeling

4.1. Muscle segment

C. elegans with a simply cylindrical body is about 1 mm in length. The body wall muscles can be classified into 4 quadrants on the transverse plane: dorsal-left (DL), ventral-left (VL), ventral-right (VR), and dorsal-right (DR). These body wall muscle cells are arranged as pairs located in four quadrants along the body, shown as the rectangles in Fig. 2(a). During locomotion, *C. elegans* lies aside (uses the left or right side touching the ground) and moves over a surface by propagating dorsal/ventral flexures along its body [41]. Based on the neuronal and muscular structure, the body of *C. elegans* is represented as a multi-joint rigid link system with 12 joints and 11 links, as shown in Fig. 2(b). The center of each

muscle segment in Fig. 2(a) is depicted as a joint in Fig. 2(b). The last three muscle segments (10, 11, 12) are combined and represented as joint 10, because anatomically the three muscle segments are controlled by only one motor neuron DB7.

4.2. Activation function

Ventral (dorsal) muscle cells receive excitatory and inhibitory inputs from VB (DB) and VD (DD) motor neurons, respectively. By following [12] the inputs to the ventral side and dorsal side muscles are

$$I_{V,i} = \sum_{j=1}^{11} w_{mVB,ij} V_{VB,j} + \sum_{j=1}^{13} w_{mVD,ij} V_{VD,j}, \tag{13}$$

$$I_{D,i} = \sum_{j=1}^{6} w_{mDD,ij} V_{DD,j} + \sum_{j=1}^{7} w_{mDB,ij} V_{DB,j}, \tag{14}$$

where $V_{VB},jV_{VD},j,V_{DD},j$ and V_{DB},j are the voltages of motor neurons VB_j, VD_j, DD_j and DB_j, respectively. $w_{mVB,ij}, w_{mVD,ij}, w_{mDD,ij}$ and $w_{mDB,ij}$ are the connection weights from neurons VB_j, VD_j, DD_j and DB_j to muscle cell i, respectively.

The activation states of muscles are represented by the variable $A^{D}_{M,i}$ and $A^{V}_{M,i}$ for the dorsal side and ventral side muscles in segment i, respectively [12],

$$\tau_M \frac{dA^{(D,V)}_{M,i}}{dt} = I_{(V,D),i} - A^{(D,V)}_{M,i}, \tag{15}$$

where τ_M is the time constant, and $I_{(V,D),i}$ comes from Eqs. (13) and (14). The activation states of muscles decide the muscle lengthes, which are represented as

$$l_{D,i} = l_0 + \sigma_L(A^{D}_{M,i}), \tag{16}$$

$$l_{V,i} = l_0 + \sigma_L(A^{V}_{M,i}), \tag{17}$$

where $l_{D,i}$ and $l_{V,i}$ are the lengths of muscles in segment i on the dorsal side and ventral side, respectively. l_0 is the muscle length when relaxing.

The muscle activation function $\sigma_L(\cdot)$ is

$$\sigma_L(x) = \frac{A_L}{1+\exp(-k_L(x-A^0_M))} + b_L, \tag{18}$$

where A_L, k_L, A^0_M and b_L are constants that should be determined and their values are provided in Section 5.

4.3. Shape changing

In this chapter, the body of *C. elegans* is divided into 10 segments according to the muscle structure and represented as a multi-joint rigid link system with 12 joints and 11 links, as shown in Fig. 2(b). Each muscle segment without shape changing is shown in Fig. 4(a). During locomotion, the muscle segment will change its shape, as shown in Fig. 4(b). Thus, we need to explore how the body shape changing influences the joint angle θ.

As shown in Fig. 4(a), for the segment i, the dorsal side muscle is $l_{D,i}$ in length and the ventral side muscle is $l_{V,i}$ in length, represented as $A'C'$ and $A''C''$, respectively. The original lengths of $l_{D,i}$ and $l_{V,i}$ are equal to l_0. During locomotion, muscles change their lengths. Let the length of each link be l_0, so in Fig. 4(b) $|AB| = l_0/2$ and $|A'A| = d/2$. It can be proved that $\angle DBC = \angle A'OB' = \theta_i$, and drawing $D'A // B'B$ yields $\angle A'AD' = \theta_i$ and $|AB| = |D'B'| = l/2$. Thus,

$$\begin{aligned} l_{D,i} &= |\widehat{A'C'}| = 2|\widehat{A'B'}| \\ &= 2(|\widehat{A'D'}| + |\widehat{D'B'}|) \\ &= 2\left(\frac{d}{2}\theta_i + \frac{l_0}{2}\right) \\ &= l_0 + d\theta_i. \end{aligned} \tag{19}$$

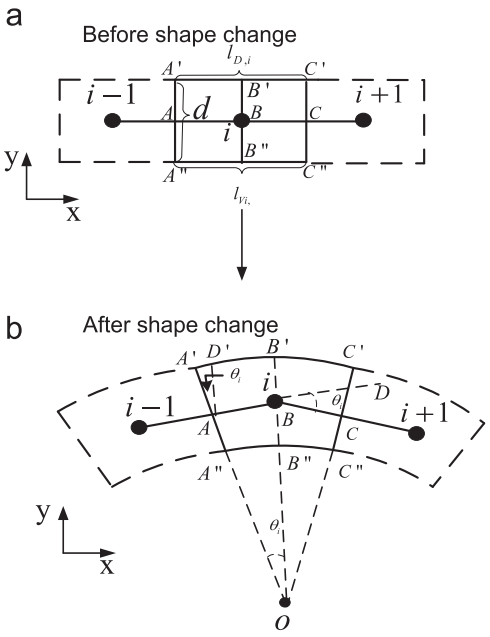

Fig. 4. (a) One body segment without shape changing. (b) One body segment with shape changing.

Following the same way, the relation between $l_{V,i}$ and θ_i is

$$l_{V,i} = l_0 - d\theta_i. \tag{20}$$

After resolving Eqs. (19) and (20), we obtain

$$\theta_i = \frac{l_{D,i} - l_{V,i}}{2d}. \tag{21}$$

From Eq. (21), we can observe that the joint angle θ_i is determined by the difference of muscle length between the dorsal and ventral muscles. Furthermore, $l_{D,i}$ and $l_{V,i}$ are determined by the outputs of motor neurons, referring Eqs. (13)–(17). Once the connection weights from motor neurons to muscles are determined, the muscles will change their lengths according to the outputs of the motor neurons.

5. Optimization and parameter setting

5.1. Body optimization

Because of the complicated neuronal and neuromuscular connections, as shown in Figs. 1 and 2, our first step is to simplify the wire diagram. From the neuromuscular structure, we assume that in the same muscle segment two ventral side (dorsal side) muscles are controlled by one motor neuron and the neuromuscular connections are listed in Table 1. As discussed in Section 4.1, we use 10 joints (refer to Fig. 2(b)) to represent the 12 muscle segments. The joint 10 represents the last three muscle segments since only one B-type motor neuron (DB7) controls these dorsal side muscles, as shown in Fig. 2.

To propagate the undulatory wave from head to tail, the motor neurons receive the curving status of their anterior muscles and active their connected muscles in current muscle segment. The curving status of muscles in the current segment can be sensed by the posterior motor neurons, which active the posterior muscles. In this way, the undulatory wave could be translated. For

Table 1
Neuromuscular connection.

Joint	Muscle segment	Ventral muscle controlled by	Dorsal muscle controlled by
1	1	RMDV	RMDD
2	2	SMBV	SMBD
3	3	SMDV	SMDD
4	4	VB1 VD1 VD2	DB1 DD1
5	5	VB2 VD3	DB2 DD2
6	6	VB3 VD4	DB3 DD3
7	7	VB4 VB5 VD5 VD6	DB4 DD4
8	8	VB6 VB7 VD7 VD8	DB5
9	9	VB8 VB9 VD9 VD10	DB6 DD5
10	10, 11, 12	VB10 VB11 VD11 VD12 VD13	DB7 DD6

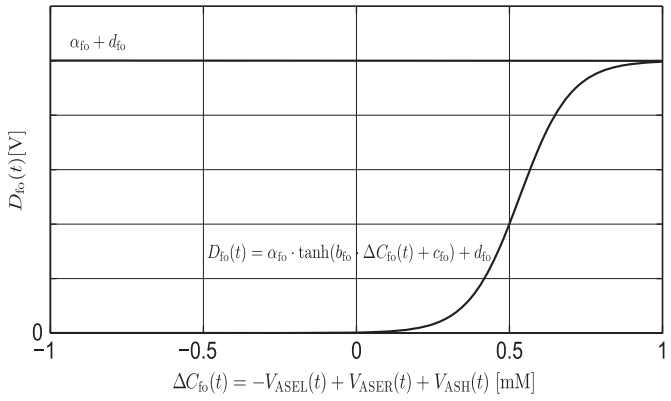

Fig. 5. SLF for the chemotaxis behavior of *C. elegans*.

simplification, in our model each motor neuron for segment i only receives the curving status of muscles in segment $i-1$.

5.2. Head optimization

The head wire diagram in our model generates the undulatory wave and the turning signal that are transmitted to the motor neurons. Three sensory neurons (ASEL, ASER, ASH) as the input neurons receive the food (ASEL and ASER) and toxin (ASH) concentrations. ASEL and ASH are *on-cells*, whereas ASER is *off-cell*.

The outputs of three sensory neurons will be transmitted to their connected interneurons and finally to the motor neurons. In our model, the head wire diagram is a three-layer DNN. The input layer contains three sensory neurons and output layer contains two motor neurons (RMDV, RMDD). Except for three interneurons (RIG, URY, RIB) that function as an undulatory wave generator, other interneurons form the second layer. We use Eq. (9) to be the activation function of these interneurons.

To achieve the decision making for chemotaxis, we construct the SLF to represent the chemotaxis behavior of *C. elegans*, as shown in Fig. 5. SLF for finding food and avoiding toxin is

$$D_{fo}(t)=\alpha_{fo}\cdot\tanh(b_{fo}\cdot\Delta C_{fo}(t)+c_{fo})+d_{fo}, \tag{22}$$

where $D_{fo}(t)$ is the desired output of SLF. $\alpha_{fo}, b_{fo}, c_{fo}$ and d_{fo} are parameters to control the shape of SLF.

$$\Delta C_{fo}(t)=-V_{ASEL}(t)+V_{ASER}(t)+V_{ASH}(t), \tag{23}$$

where $V_{ASEL}(t), V_{ASER}(t)$ and $V_{ASH}(t)$ are outputs of sensory neurons ASEL, ASER and ASH at time t, respectively. Biologically, ASEL and ASER cannot active at the same time [22–24]. For food attraction, when *C. elegans* is towards the correct direction, *on-cell* ASEL will active to be a positive value $V_{ASEL}(t)$. $-V_{ASEL}(t)$ is a negative value that suppresses the output of $D_{fo}(t)$ to be zero, as shown in Fig. 5. Contrarily, when *C. elegans* is towards the wrong direction, *off-cell* ASER will be activated to a positive value, which generates a turning signal to the motor neurons. For avoiding toxin, once the temporal toxin concentration difference is greater than zero, $V_{ASH}(t)$ is a positive value, which generates the turning signal since $D_{fo}(t)>0$.

There are several kinds of algorithms can be adopted to train DNN, such as Evolutionary Computation and Particle Swarm Optimization. In this work we use Differential Evolution (DE) directly by following our previous work [20]. DE is one of the powerful stochastic real-parameter optimization algorithms and it operates through similar computational steps as a standard evolutional algorithm. Furthermore, the DE toolbox is available for several softwares and can be modified and applied easily.

For each training data there are three inputs with range $[-2,2]$ and two outputs with the range [0,1]. The three inputs stand for the three sensory neurons (ASEL, ASER, ASH) and two outputs stand for the two motor neurons (RMDV, RMDD). For the optimization criteria, we define the cost function as

$$cost(x_i)=\frac{1}{2}\sum_{k=1}^{N_t}\left[D_{OUT,i}(k)-V_{OUT,i}(k)\right]^2, \tag{24}$$

where x_i denotes the ith chromosome. N_t is the number of training data. We define $D_{OUT,i}(k)=[D_{fo}(k), -D_{fo}(k)]$ as the ith chromosome with the kth input data. Two terms $D_fo(k)$ and $-D_{fo}(k)$ indicate the desired outputs of neurons RMDV and RMDD with the kth input data. The reason of setting two terms of D_{OUT} to be opposite signals is that RMDV and RMDD control two opposite muscles in the same segment, and the opposite signals of two motor neurons in the same segment are critical to generate the undulatory wave. D_{fo} can be calculated from Eq. (22), and ΔC_{fo} can be calculated from Eq. (23). Finally, $V_{OUT,i}(k)$ is the actual outputs of RMDV and RMDD for the ith chromosome with the kth input data. Except for the optimization criteria, other operations such as the *mutation, crossover, selection* and the whole procedure of DE are same to those in Ref. [20]. The DE toolbox of Matlab is adopted directly in our work.

5.3. Other parameter setting

Except for the parameters obtained by DE, other parameters are obtained by trial and error, which are listed in Table 2.

6. Results

In this section, we first test the chemotaxis behavior of our model for finding food and avoiding toxin in different scenarios. Second, the trajectories of our model are analyzed quantitatively by comparing with the experiment results. Last, the well trained wire diagrams are simplified and two patterns are found.

6.1. Concentration distribution

In the simulated environments for testing, the concentration distribution for food or toxin is assumed in Gaussian distribution, as shown in Fig. 6,

$$C(x,y)=C_{max}\exp\left(-\frac{x^2+y^2}{S}\right), \tag{25}$$

where C_{max} is the peak value of food or toxin concentration and S is the variance of the distribution. The unit of the concentration $C(x,y)$ is millimolar concentration (mmol/L, short for mM).

Table 2
Parameters setting.

Parameter	Value	Description
M	1 s	Time duration in Eq. (1)
N	1 s	Time duration in Eq. (2)
A	1	Magnitude of activation function in Eq. (3)
k_s	6.5	Steepness of activation function in Eq. (3)
x_0	−1	Constant in activation function Eq. (3)
τ_{RIG}	2	Time constant in Eq. (6)
τ_{RIB}	2	Time constant in Eq. (6)
τ_{URY}	0	Time constant in Eq. (6)
C_B	0.01	Time constant for motor neuron in Eq. (10)
G_B	1	Membrane conductance in Eq. (10)
E_{rev}	0	Constant for cell's potential in Eq. (10)
A_p	43.5	Magnitude of activation function for proprioceptive feedback in Eq. (11)
k_p	0.2	Steepness of activation function for proprioceptive feedback in Eq. (11)
l_0	1 mm	Original muscle length in Eqs. (11), (16) and (17)
b_p	−21.75	Constant for proprioceptive feedback activation function in Eq. (11)
τ_M	0.01	Time constant for muscle activation function in Eq. (15)
A_L	9.23	Magnitude of muscle activation function in Eq. (18)
k_L	0.2	Steepness of muscle activation function in Eq. (18)
A_M^0	0	Constant for muscle activation function in Eq. (18)
b_L	−4.62	Constant for muscle activation function in Eq. (18)
C_{max}	2	Peak value of concentration in Eq. (25)
S	10	Variance of concentration distribution in Eq. (25)
α_{fo}	0.5	Parameters for the magnitude of SLF in Eq. (22)
b_{fo}	6	Parameters for the steepness of SLF in Eq. (22)
c_{fo}	2.7	Parameters for the location of SLF in Eq. (22)
d_{fo}	0.5	Parameters for the location of SLF in Eq. (22)

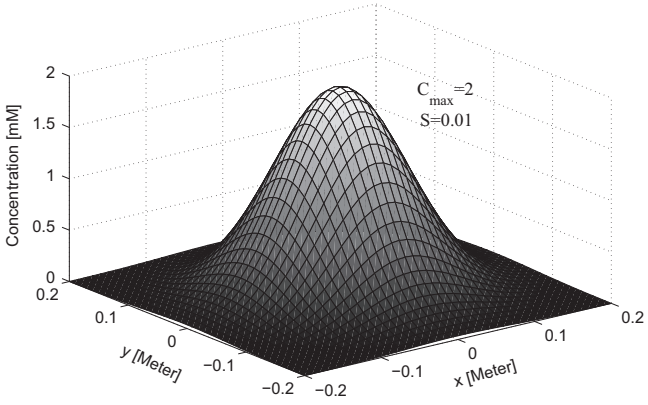

Fig. 6. Concentration distribution.

6.2. Chemotaxis behavior

To test the chemotaxis behavior of our model, we put it into three different scenarios: (1) only one food source existed, (2) both food and toxin existed with concentration slightly overlapped and (3) heavily overlapped.

6.2.1. One food source

As shown in Fig. 7, one food source is located at (0,0) with Gaussian distribution. *C. elegans* starts at four different locations, (20,60), (57,28), (−20,−40) and (−42,−14), respectively. It moves towards the food source and finally arrives at it. From the resting result, we can observe that *C. elegans* has successfully achieved the task of finding food.

6.2.2. Food and toxin concentrations slightly overlapped

To test whether our model can perform the task of finding food and avoiding toxin simultaneously, we construct the scenario with nine sources distributed as a 3 × 3 grid. As shown in Fig. 8, except

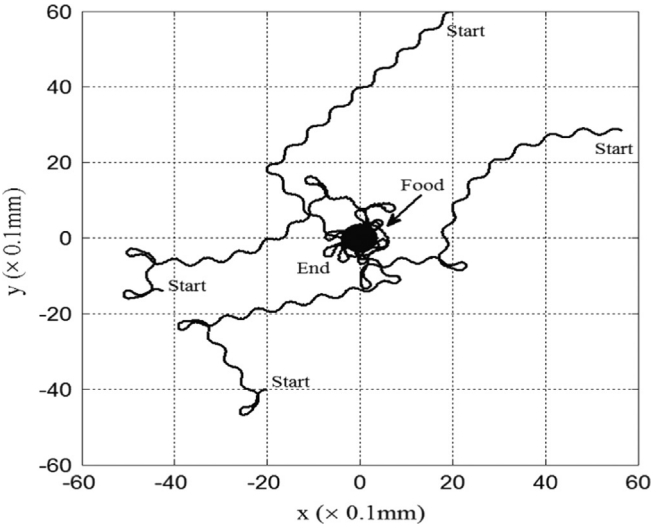

Fig. 7. Testing result in the scenario that only one food is existed.

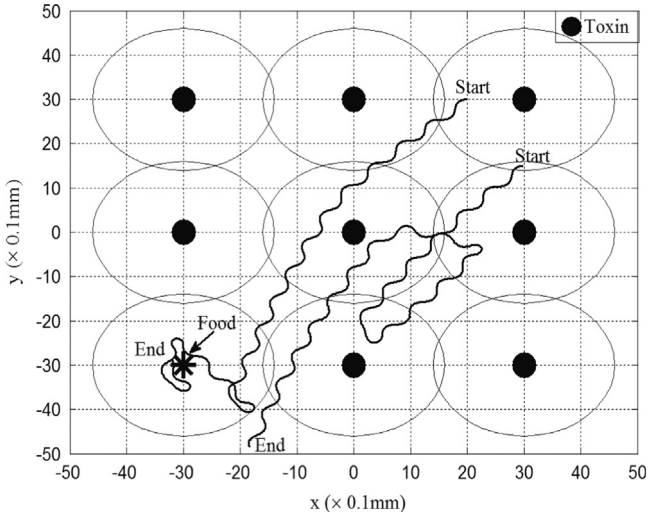

Fig. 8. Testing result in the scenario that food and toxin concentrations are slightly overlapped.

for the asterisk located at (−30,−30) denotes the food source, other eight dots denote the toxin sources. The circle lines are the boundaries of food and toxin concentrations. In the test, *C. elegans* starts at two different locations (30,15) and (20,30), respectively. From the trajectory starting from (30,15), it is obvious that *C. elegans* escapes from the toxin and finally settles down at the place where no toxin concentration exists. When starting from (20,30), *C. elegans* escapes from the toxin sources first. Once it smells the food concentration, it moves towards the food source and finally surrounds it.

6.2.3. Food and toxin concentrations heavily overlapped

In this test, we construct the scenario in which one food source and one toxin source are located at (−30,0) and (30,0), respectively, with concentrations largely overlapped, as shown in Fig. 9. When the food and toxin concentrations overlap heavily, the best place for the worm is (−65.72,0), which is obtained by solving $\nabla C_f = \nabla C_{tx}$, where $\nabla C_f = (\partial C_f/\partial x)\hat{i} + (\partial C_f/\partial y)\hat{j}$ and $\nabla C_{tx} = (\partial C_{tx}/\partial x)\hat{i} + (\partial C_{tx}\partial y)\hat{j}$.

When starting from the point (−150,0), *C. elegans* moves towards the food and finally settles down around the target place at (−65.72,0) (track A). When *C. elegans* starts from (10,90), where both food and toxin concentrations exist, it avoids the toxin and

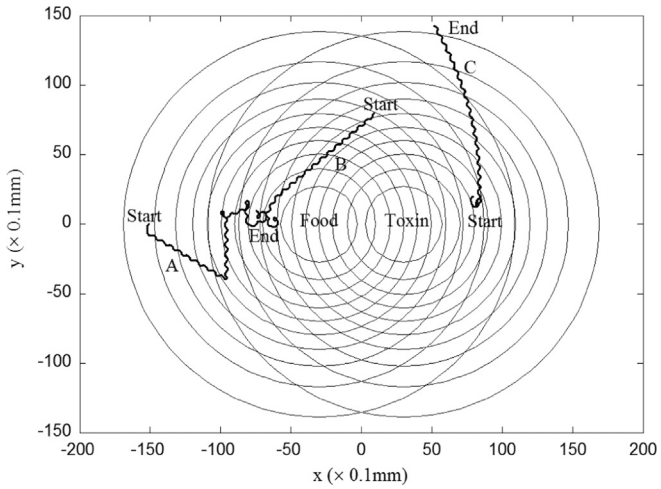

Fig. 9. Testing result in the scenario that food and toxin concentrations are heavily overlapped.

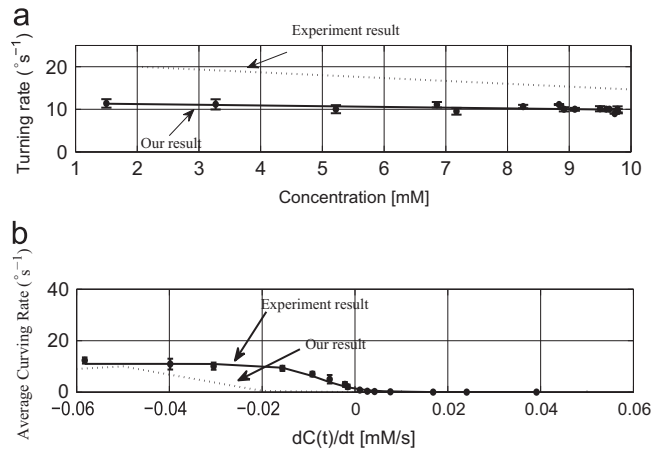

Fig. 10. Quantitative analysis of the trajectories for food attraction. (a) The relation between turning rate and concentration. (b) The relation between average curving rate and $dC(t)/dt$.

approaches the food. Finally, it settles down at the target place $(-65.72,0)$ (track B). When starting from the point (60,20), where both toxin and food concentrations exist, *C. elegans* avoids the toxin and navigates itself faraway from the toxin source. Finally, it settles down at the place without toxin concentration (track C).

6.3. Quantitative analysis

To analyze the performance of our model, we provide the quantitative analysis of the trajectories for food attraction by comparing other work [34,42], in which the biological experiments are conducted for the behavior of *C. elegans* to attractants.

We investigate the relations between: (1) turning rate and concentration; (2) average curving rate and $dC(t)/dt$. The result is shown in Fig. 10.

In Fig. 10(a) we can observe the turning rate weakly depends on the food concentration (solid line), and it is similar to the experiment result (dashed line) [42]. The relation between average curving rate and $dC(t)/dt$ is shown in Fig. 10(b) (solid line). In this figure, the larger negative value of $dC(t)/dt$ yields the larger magnitude of curving rate. However, once $dC(t)/dt$ is positive, the curving rate reduces to zero. This result has the same trend to the experiment data (dotted line) [34].

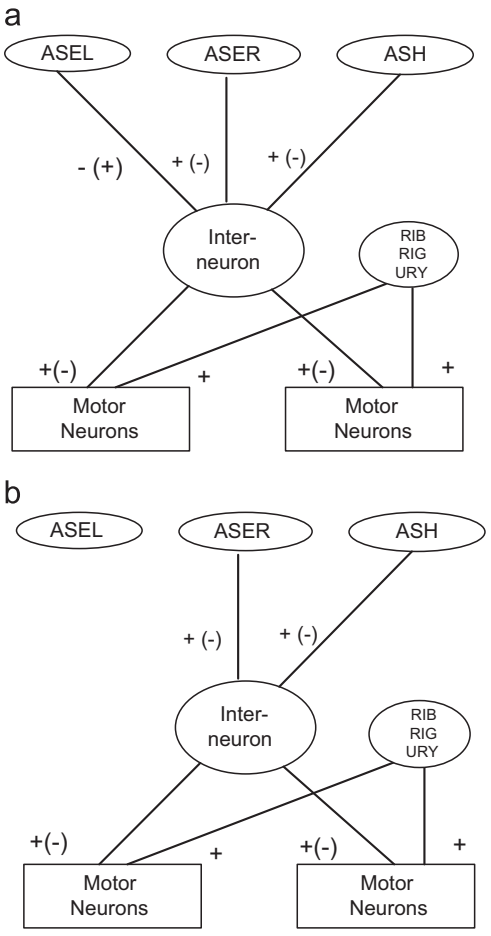

Fig. 11. (a) The first pattern contains three sensory neurons. (b) The second pattern contains two sensory neurons.

6.4. Wire diagram patterns

We simplify the well trained head wire diagrams by following the method in [43] and find out two patterns, as shown in Fig. 11 (a) and (b), respectively.

The difference between two patterns is that in pattern A there exists the connection between ASEL and interneuron, whereas in pattern B, this connection is extremely weak and even eliminated. However, wire diagrams for both patterns can achieve the same task as finding food and avoiding toxin. Our result corresponds with the experimental result that the chemotaxis behavior of *C. elegans* is not impaired heavily after ASEL is ablated [44]. Furthermore, there exist two sub-patterns within either pattern A or B. The difference between two sub-patterns is the opposite signs (symbols in the parentheses) of the weights from sensory neurons to motor neurons.

7. Discussion and conclusion

Before closing this paper, some discussions should be pointed out. Firstly, this work mainly investigated the undulatory locomotion of *C. elegans* based on the biological neural wire diagram and muscle structure. The objective of this work focuses on the neuromuscular mechanism to generate the undulatory locomotion. Thus, we did not compare and test different learning methods. Secondly, the supervised learning method is adopted in this work instead of unsupervised learning. In a sense, the supervised learning is relatively not biological plausible since the nature

worm has no teachers. However, it is still an effective way to explore the biological properties of *C. elegans* by using the supervised learning methods since the unsupervised learning methods for DNN are very limited. Thirdly, it should be pointed out that the biologically plausible structures of the network can be obtained through different ways. Not only we can use the heuristic methods such as evolutionary computing and artificial neural networks, but also the traditional algorithm such as the graph theory and so on. Whatever the methods chosen in this kind of work, we must follow the biological truth of the organism without arbitrarily assuming and thinking.

Above all, this work has developed an undulatory locomotion model that can perform the chemotaxis behavior of finding food and avoiding toxin concurrently. The undulatory locomotion model can mimic the whole body movement of *C. elegans* instead of considering it as a point. The *on-cell* and *off-cell* mechanism is incorporated for the sensory neurons, as well as the proprioceptive mechanism for the motor neurons. The *on-cell* and *off-cell* mechanism makes the sensory neurons work independently for the decision making of turning, and the proprioceptive mechanism makes the motor neurons have the ability to propagate the undulatory wave even the motor neurons are not fully connected biologically. Furthermore, we construct the nonlinear function to mimic the logic of chemotaxis behavior of *C. elegans* and after that we train the DNN to learn it. Once being well trained, the locomotion model can perform well in finding food and avoiding toxin in different environments. At last, the quantitative analysis is provided to verify the effectiveness of the locomotion model.

In future work, we will investigate the 3D locomotion of *C. elegans* based on the biological neural wire diagram and muscle structure. Additionally, more training methods will be explored to get more plausible networks and the worm-like robot will also be constructed according to the theoretical results.

Acknowledgments

The authors would like to thank the support from the National Natural Science Foundation of China (Nos. 61403054, 61403053), and the Fundamental and Frontier Research Project of Chongqing (Nos. cstc2014jcyjA40001, cstc2014jcyjA40022), and the Science Foundation Project of CQ Education Commission (No. KJ1400436).

References

[1] M. Chalfie, J. White, The Nervous System in the Nematode *Caenorhabditis elegans*, 1st edition, Cold Spring Harbor Laboratory, New York, 1998.
[2] I. Erkmen, A.M. Erkmen, F. Matsuno, R. Chatterjee, T. Kamegawa, Snake robots to the rescue! Robot. Autom. Mag. 9 (2002) 17–25.
[3] R.J. Webster, J.M. Romano, N.J. Cowan, Mechanics of precurved-tube continuum robots, IEEE Trans. Robot. 25 (2009) 67–78.
[4] J. Borenstein, A. Borrell, The OmniTread OT-4 serpentine robot, In: Proceedings of IEEE International Conference on Robotics and Automation, 2008.
[5] S. Manzoor, Y. Choi, A unified neural oscillator model for various rhythmic locomotions of snake-like robot, Neurocomputing 173 (2016) 1112–1123.
[6] A. Degani, H. Choset, A. Wolf, M.A. Zenati, Highly articulated robotic probe for minimally invasive surgery, In: Proceedings of IEEE International Conference on Robotics and Automation, 2006.
[7] M. Suzuki, T. Tsuji, H. Ohtake, A model of motor control of the nematode *C. elegans* with neuronal circuits, Artif. Intell. Med. 35 (2005) 75–86.
[8] M. Suzuki, T. Tsuji, H. Ohtake, A dynamic body model of the nematode *C. elegans* with a touch-response circuit, In: Proceedings of the IEEE International Conference on Robotics and Biomimetics (ROBIO), 2005, pp. 538–543.
[9] M. Suzuki, T. Goto, T. Tsuji, H. Ohtake, A motor control model of the nematode *C. elegans*, In: Proceedings of IEEE International Conference on Robotics and Biomimetics, 2005.
[10] M. Suzuki, T. Tsuji, H. Ohtake, A neuromuscular model of *C. elegans* with directional control, In: Proceedings of the First International Conference on Complex Medical Engineering, 2004, pp. 167–172.
[11] J.H. Boyle, J.A. Bryden, N. Cohen, An integrated neuro-mechanical model of *C. elegans* forward locomotion, Lect. Notes Comput. Sci. 4984 (2008) 37–47.
[12] J.H. Boyle, N. Cohen, *Caenorhabditis elegans* body wall muscles are simple actuators, Biosystems 94 (2008) 170–181.
[13] J.H. Boyle, S. Johnson, A.A. Dehghani-Sanij, Adaptive undulatory locomotion of a *C. elegans* inspired robot, IEEE/ASME Trans. Mech. 18 (2013) 439–448.
[14] J. Karbowski, G. Schindelman, C.J. Cronin, A. Seah, P.W. Sternberg, Systems level circuit model of *C. elegans* undulatory locomotion: mathematical modeling and molecular genetics, J. Comput. Neurosci. 24 (2008) 253–276.
[15] R. Mailler, J. Avery, J. Graves, N. Willy, A biologically accurate 3D model of the locomotion of *Caenorhabditis Elegans*, In: Proceedings of the International Conference on Biosciences, 2010, pp. 84–90.
[16] H. Yuk, J.H. Shin, S. Jo, Design and control of thermal sma based small crawling robot mimicking *C. elegans*, In: Proceedings of the IEEE International Conference on Intelligent Robots and Systems, 2010, pp. 407–412.
[17] H. Yuk, D. Kim, H. Lee, S. Jo, J.H. Shin, Shape memory alloy-based small crawling robots inspired by *C. elegans*, Bioinspir. Biomim. 6 (2011) 046002.
[18] J.X. Xu, X. Deng, Study on chemotaxis behaviors of *C. elegans* using dynamic neural network models: from artificial to biological models, J. Biol. Syst. 18 (2010) 3–33.
[19] J.X. Xu, X. Deng, Biological modeling of complex chemotaxis behaviors for *C. elegans* under speed regulation-Dynamic Neural Networks approach, J. Comput. Neurosci. 35 (2013) 19–37.
[20] J.X. Xu, X. Deng, A 3D undulatory locomotion model inspired by *C. elegans* through DNN approach, Neurocomputing 131 (2014) 248–264.
[21] T.E. Portegys, Training sensory-motor behavior in the connectome of an artificial *C. elegans*, Neurocomputing 168 (2015) 128–134.
[22] T.R. Thiele, S. Faumont, S.R. Lockery, The neural network for chemotaxis to tastants in *Caenorhabditis elegans* is specialized for temporal differentiation, J. Neurosci. 29 (2009) 11904–11911.
[23] E.J. Izquierdo, S.R. Lockery, Evolution and analysis of minimal neural circuits for klinotaxis in *Caenorhabditis elegans*, J. Neurosci. 30 (2010) 12908–12917.
[24] S. Faumont, T.H. Lindsay, S.R. Lockery, Neuronal microcircuits for decision making in *C. elegans*, Curr. Opin. Neurobiol. 22 (2012) 580–591.
[25] Q. Wen, M.D. Po, E. Hulme, S. Chen, X. Liu, S.W. Kwok, M. Gershow, A.M. Leifer, V. Butler, C. Fang-Yen, T. Kawano, W.R. Schafer, G. Whitesides, M. Wyart, D. B. Chklovskii, M. Zhen, A.D.T. Samuel, Proprioceptive coupling within motor neurons drives *C. elegans* forward locomotion, Neuron 76 (2012) 750–761.
[26] D.A. Weisblat, R.L. Russell, Propagation of electrical activity in the nerve cord and muscle syncytium of the nematode *Ascaris lumbricoides*, J. Comp. Physiol. A: Neuroethol. Sens. Neural Behav. Physiol. 107 (1976) 293–307.
[27] B.L. Chen, D.H. Hall, D.B. Chklovskii, Wiring optimization can relate neuronal structure and function, Proc. Natl. Acad. Sci. U. S. A. 103 (2006) 4723–4728.
[28] A.M. Shaw, F.J. Doyle III, J.S. Schwaber, A dynamic neural network approach to nonlinear process modeling, Comput. Chem. Eng. 21 (1997) 371–385.
[29] WormAtlas, ⟨(http://www.wormatlas.org/)⟩.
[30] WormWeb, ⟨(http://www.wormweb.org/)⟩.
[31] C.T. Bargmann, H.R. Horvitz, Chemosensory neurons with overlapping functions direct chemotaxis to multiple chemicals in *C. elegans*, Neuron 7 (1991) 729–742.
[32] J.M. Gray, J.J. Hill, C.I. Bargmann, A circuit for navigation in *Caenorhabditis elegans*, Proc. Natl. Acad. Sci. U. S. A. 102 (2005) 3174–3191.
[33] J.G. White, E. Southgate, J.N. Thomson, S. Brenner, The structure of the nervous system of the nematode *Caenorhabditis elegans*, Philos. Trans. R. Soc. B: Biol. Sci. 314 (1986) 1–340.
[34] Y. Iino, K. Yoshida, Parallel use of two behavioral mechanisms for chemotaxis in *Caenorhabditis elegans*, J. Neurosci. 29 (2009) 5370–5380.
[35] H. Sasakura, I. Mori, Behavioral plasticity, learning, and memory in *C. elegans*, Curr. Opin. Neurobiol. 23 (2013) 92–99.
[36] E.L. Ardiel, C.H. Rankin, Some like it hot: decoding neurotransmission in the worm's thermotaxis circuit, EMBO J. 30 (2011) 1192–1194.
[37] J.Q. White, E.M. Jorgensen, Sensation in a single neuron pair represses male behavior in hermaphrodites, Neuron 75 (2012) 593–600.
[38] S.H. Chalasani, S. Kato, D.R. Albrecht, T. Nakagawa, L.F. Abbott, C.I. Bargmann, Neuropeptide feedback modifies odor-evoked dynamics in *Caenorhabditis elegans* olfactory neurons, Nat. Neurosci. 13 (2010) 615–621.
[39] M.B. Goodman, D.H. Hall, L. Avery, S.R. Lockery, Active currents regulate sensitivity and dynamic range in *C. elegans* neurons, Neuron 20 (1998) 763–772.
[40] J.A. Bryden, N. Cohen, Neural control of *Caenorhabditis elegans* forward locomotion: the role of sensory feedback, Biol. Cybern. 98 (2008) 339–351.
[41] D.L. Riddle, T. Blumenthal, B.J. Meyer, J.R. Preiss (Eds.), *C. elegans* II, Cold Spring Harbor Laboratory Press, NY, 1997.
[42] J.T. Pierce-Shimomura, T.M. Morse, S.R. Lockery, The fundamental role of pirouettes in *Caenorhabditis elegans* chemotaxis, J. Neurosci. 19 (1999) 9557–9569.
[43] N.A. Dunn, A novel neural network analysis method applied to biological neural networks (Ph.D. thesis), University of Oregon, OR, USA, 2006.
[44] H. Suzuki, T.R. Thiele, S. Faumont, M. Ezcurra, S.R. Lockery, W.R. Schafer, Functional asymmetry in it *Caenorhabditis elegans* taste neurons and its computational role in chemotaxis, Nature 454 (2008) 114–117.

Xin Deng received the Bachelors degree from Department of Computer Science and Technology, Jilin University, Changchun, China, in 2004, and Masters degree from Department of Computer Science, Chongqing University, Chongqing, China, in 2007. He was awarded the Ph.D. degree in computer engineering from National University of Singapore, Singapore, in 2013. He is now an associate professor in College of Computer Science and Technology, Chongqing University of Posts and Telecommunications in China.

Jian-Xin Xu received the Bachelors degree in electrical engineering from Zhejiang University, Hangzhou, China, in 1982, and the Masters and Ph.D. degrees in electrical engineering from the University of Tokyo, Tokyo, Japan, in 1986 and 1989, respectively.

He spent one year at the Hitachi Research Laboratory, Ibaraki, Japan, more than one year in Ohio State University, Columbus, as a Visiting Scholar, and 6 months in Yale university, New Haven, CT, as a Visiting Research Fellow. He joined the National University of Singapore, Singapore, in 1991, and is currently a Professor at the Department of Electrical Engineering. He is entitled as the *IEEE Fellow* since January 2012. His current research interests include learning theory, intelligent control, nonlinear and robust control, robotics, and precision motion control.

Jin Wang obtained his bachelor degree in 2001 in Electrical Engineering and Automation, Xian Jiaotong University, China. He was awarded the Ph.D degree in 2008 in Information & Communication Engineering, Inha University, Korea. Now he is the professor in School of Computer Science and Technology, Chongqing University of Posts and Telecommunications, China. His research interests include Digital System Design, Evolutionary Computation, Evolvable Hardware, Bio-inspired Hardware, DNA Computing, Bioinformatics.

Guo-yin Wang received the bachelors degree in computer software, the masters degree in computer software, and the Ph.D. degree in computer organization and architecture from Xian Jiaotong University, Xian, China, in 1992, 1994, and 1996, respectively. He is the professor and the head of School of Computer Science and Technology, Chongqing University of Posts and Telecommunications, China. He is the Director of the Institute of Electronic Information Technology, Chongqing Institute of Green and Intelligent Technology, CAS, China. He is also a part-time professor with the Southwest Jiaotong University, Xian Jiaotong University, Shanghai Jiaotong University, Xidian University, and University of Electronic Science and Technology of China. His research interests include rough set, granular computing, knowledge technology, data mining, machine learning, neural network, soft computing, cognitive computing, etc.

Qiao-song Chen obtained his bachelor degree in 2001 in Electrical Engineering and Automation, Xian Jiaotong University, China. He was awarded the PhD degree in 2011 in Information & Communication Engineering, Inha University, Korea. Now he is the associate professor in School of Computer Science and Technology, Chongqing University of Posts and Telecommunications, China. His research interests include Image Processing, Pattern Recognition, Computer Vision.